Exp Fluids (2006) 41:869–880
DOI 10.1007/s00348-006-0202-1

RESEARCH ARTICLE

# Statistical particle tracking velocimetry using molecular and quantum dot tracer particles

**Jeffrey S. Guasto · Peter Huang · Kenneth S. Breuer**

Received: 21 December 2005 / Revised: 28 July 2006 / Accepted: 7 August 2006 / Published online: 13 September 2006


**Abstract** We present a statistical approach to particle tracking velocimetry developed to treat the issues associated with nanometer-sized tracer particles such as fluorescent molecules and quantum dots (QDs) along with theory and experimental results. Extremely small tracers pose problems to traditional tracking methods due to high levels of thermal motion, high levels of intensified camera noise, high drop-in/drop-out rates and, in the case of QDs, fluorescence intermittency (‘‘blinking’’). The algorithm presented here compensates for these problems in a statistical manner and determines the physical velocity distributions from measured particle displacement distributions by statistically removing randomly distributed, non-physical tracking events. The algorithm is verified with both numerically simulated particle trackings and experiments using 54 nm diameter fluorescent dextran molecules and 6 and 16 nm diameter QDs.

## 1 Introduction

Particle image velocimetry (PIV) and particle tracking velocimetry (PTV) have become integral techniques in experimental fluid mechanics. Originally developed for macroscale measurements, these velocimetry methods have evolved to suit applications in microscale fluid mechanics ($\mu$PIV and $\mu$PTV). Both techniques employ the use of tracer particles suspended in a fluid of interest along with digital cameras to capture successive images of particle position in the fluid through time. PIV uses cross-correlation algorithms to determine the most probable spatial displacement for an interrogation region (IR) within an image pair (Adrian 1991). High density particle seeding and low diffusivity is preferable to increase accuracy. PTV methods, on the other hand, typically track single particles and use particle center detection with nearest-neighbor matching to determine the most probable single particle displacement (Schmidt et al. 1996). For PTV, low particle seeding density is necessary to ensure one-to-one tracking between IRs.

As we approach the nanoscale in fluid mechanics, Brownian motion, camera noise and the desire for higher tracer particle seeding make traditional PTV methods difficult to implement. Brownian motion increases as tracer particle diameter decreases, resulting in large variations in the measured velocity, even for a ‘‘steady’’ flow. In addition, thermal motion leads to high particle drop-out, in which particles observed in the first IR of an image pair are lost from the subsequent IR. Since CCD cameras are limited by a finite exposure time and image pair separation time, IRs must be chosen to cover a relatively large image area to adequately capture a significant number of tracer particles that would otherwise drop-out within that time. Large IRs and/or dense tracer particle concentrations result in the gross mismatching of tracer particles, which is a major problem for PTV methods that rely on one-to-one tracking.

J. S. Guasto (✉) · P. Huang · K. S. Breuer
Division of Engineering, Brown University,
Providence, RI 02912, USA
e-mail: jguasto@brown.edu

Nanometer-sized tracers also have a significantly lower image intensity than tracer particles measuring several hundred nanometers, which requires experiments to push the detection limits of intensified CCD (ICCD) cameras. High intensifier gain produces significant shot noise and intensifier noise, much of which is easily rejected through imaging optimization and image processing. However, at high intensifier gain, ICCD cameras can produce noisy artifacts due to effects like blooming and cross-talk (Burke 1996), which can appear similar in shape, size and intensity profile to real tracer particles. This intensifier noise is often indistinguishable from a tracer particle's diffraction-limited spot, and consequently, may be misconstrued as a real particle by a PIV/PTV algorithm. This leads to another source of tracking error—false particle images.

Nanoparticles themselves also introduce unique problems for tracking algorithms. Semiconductor nanocrystals or quantum dots (QDs) are promising new nanofluidic tracer particles (Bausch and Weitz 2002; Pouya et al. 2005). Although, they exhibit several qualities beneficial for nano-velocimetry (small diameter, tunable wavelength, variable surface coating), their high diffusivity makes them difficult to track. Also, they experience fluorescence intermittency or "blinking," which results in periods of fluorescence and dormancy on time scales ranging from sub-milliseconds to hours (Nirmal et al. 1996). We discuss the effects of this phenomena on tracking algorithms and show that it can be interpreted as an additional optical drop-in/drop-out.

In order to address these issues, we present a statistical particle tracking method, which is similar in principle to traditional PTV algorithms, but resolves all of the above-mentioned problems. The technique deliberately measures velocity distributions (rather than a single velocity), and utilizes a large search window to purposely include multiple tracer particles. Drop-in/drop-out particles, blinking particles and extraneous intensifier noise signals are all included in the tracking, and later eliminated from the velocity distribution by exploiting their statistical nature. The algorithm is validated both experimentally, by tracking single molecules and QDs, and with a particle tracking simulation. The remainder of the paper is organized as follows: the next section discusses the statistical tracking algorithm, including a theory for particle drop-out, proposed statistical techniques for removal of spurious tracking due to intensifier noise, drop-in/out and QD blinking, and numerical validation. Lastly, experimental validation is presented using both molecular and quantum-dot tracer particles.

## 2 Theoretical considerations

### 2.1 Principles of statistical tracking

Single particle tracking is difficult with high tracer particle concentrations, or analogously, highly diffusive tracer particles, because during any reasonable time delay, each particle can move a large enough distance (due to diffusion and/or convection) to infringe on the IR of another particle. Nearest-neighbor matching does not guarantee a correct match, and one-to-one tracking may not be possible given the need for a large IR to catch large particle displacements, which will undoubtedly include spurious particles. Consider an ideal image pair with particles in motion but no noise, no drop-in/drop-out and no blinking. In a typical PTV algorithm, the sub-pixel center locations of all individual particles are found using a thresholding and center detection scheme in both images. Next, an IR (usually square or circular) of predetermined size is centered on each individual particle in the first image and tracked to a *single* particle in the second frame, which falls within that IR. If more than one particle (or zero) is detected in the IR of the second frame, then those possible trackings must be omitted due to uncertainty. The IR size and particle seeding density must be carefully selected in conjunction with the diffusion and convection in the system to ensure one-to-one tracking, and this generally requires low seeding densities.

In the statistical particle tracking velocimetry (SPTV) algorithm, we implement a similar approach, but allow multiple particle trackings for each IR, which allows for larger IRs and higher seeding densities. A rectangular IR is constructed around each particle in the first image. The IRs need not be centered around each particle, but they should have the same orientation with respect to each particle. Next, we compute displacement vectors from the single original particle location to every particle detected within that IR in the second image. Over a given spatial region of the image where the diffusion and convection are approximately constant, we repeat this procedure for all particles and many images (several hundred), building a large distribution of particle displacements. Again, for ideal images and a sufficiently large IR, we guarantee that one displacement vector of the multiple trackings for each IR is correctly matched. All other trackings are computed from uncorrelated positions due to mismatching. Because of the manner in which we produce the IRs, the displacement distribution of the mismatched particles form a random, uniform distribution. By estimating the size of the random distribution it can be statistically subtracted from the total displacement distribution to reveal the physical displacement distribution [a similar method was first proposed by Breedveld et al. (1998)].

In practice, we must consider the effects of tracking particles which physically drop-in and drop-out of the image due to diffusion and convection, and optically drop-in and drop-out due to blinking in particles such as QDs. We will show later that these two phenomena can be treated identically. Additionally, small, low intensity tracer particles require the use of high gain ICCD cameras, which can produce random intensifier noise signals that can appear identical to tracer particles in size, shape and intensity. These intensifier noise signals can meet the detection criteria for real particle signals and are often tracked mistakenly. Thus, when we track a signal (real particle or noise) from the first image to a signal from the corresponding IR of the second image, the tracking has one of five possible meanings: (1) particle to particle (physical), (2) particle to particle (mismatch), (3) noise to particle, (4) particle to noise and (5) noise to noise tracking. Each of these phenomena make single particle tracking, and possibly PIV ensemble particle tracking less accurate due to the presence of random statistical contamination. We can easily rationalize that for a large ensemble of trackings, all non-physical trackings contribute to a random, uniform displacement distribution just as the mismatched particles in the ideal case. The reason is that at least one of the two signals is randomly located in its image with respect to the other, and thus there is no correlation between the positions of the two signals.

The SPTV technique is comparable to a method developed by Breedveld et al. (1998), who presented an algorithm that is based on the spatial correlation of all particle locations over a single IR with diffusion and convection for the purpose of measuring self-diffusion in suspensions. The method can account for physical drop-out and if it were applicable at the time, optical drop-out (blinking). However, the algorithm does not take into account random detectable signals such as those due to ICCD camera noise, which was not applicable for their experiments with large particles (tens of microns) in direct illumination. Additionally, complicated displacement distributions resulted from the choice of IR, which requires an assumed velocity profile and could not be evaluated due to dependence on other unknown functions. In practice, the authors were able to determine the shape of the particle displacement distribution through a clever symmetry argument, then extract the diffusion dynamics through a Gaussian fit of the particle displacements.

The strength of the SPTV algorithm is in considering the contributions of random noise signals and the choice of IR such that the uncorrelated trackings always form a simple random, uniform distribution. Additionally, the individually tracked particles can easily be re-binned across different regions of the image to resolve non-uniform velocities. This technique can in principle be used in systems with high particle seeding as long as individual particles are discernable for proper center detection. The average velocity and thermal motion can be extracted from the total displacement distribution function by fitting a distribution (Gaussian or otherwise). This can be done more generally through estimating the height of the random displacement distribution and subtracting the contributions of its moments from the total distribution. For this procedure, the drop-out and number of real particle signals must be estimated. A general method is critical in nanoscale systems where non-Gaussian particle motions are common [for example close to walls where hindered diffusion and shear generate asymmetric particle displacement distributions (Jin et al. 2004; Huang et al. 2006)].

## 2.2 Tracer particle diffusion and drop-out estimation

As tracer particle size decreases, the contribution of diffusion to velocity measurements becomes considerable and cannot be ignored. Here we present estimations for tracer particle diffusion and drop-out. In the fluid bulk, diffusion is isotropic and can be decoupled in all three dimensions. Additionally, we do not include coupling of convection and diffusion, since Peclet numbers tend to be quite small (less than 0.04 for our experiments). The probability that a single particle will displace a distance $\Delta z$ during a time interval $\Delta t$ typically follows a Gaussian distribution and, in one dimension, is described by

$$P(z) = \frac{1}{\sqrt{2\pi}d} \exp\left[-\frac{\Delta z^2}{2d^2}\right], \quad \text{with } d = \sqrt{2D\Delta t}, \tag{1}$$

where $d$ is the characteristic diffusion length [and the standard deviation of the probability distribution $P(z)$] and $D$ is the diffusivity. For Newtonian fluids, $D$ is accurately approximated by the Stokes–Einstein equation

$$D = \frac{k_{\mathrm{B}}T}{6\pi\mu a}, \tag{2}$$

where $k_{\mathrm{B}}$ is Boltzmann's constant, $T$ is the absolute temperature of the fluid, $\mu$ is the dynamic viscosity of the fluid and $a$ is the radius of the tracer particle.

A particle experiences out-of-plane drop-out when it diffuses along the optical axis $z$, perpendicular to the focal plane and out of the finite effective depth of field, $2h$, described by

$$h = \left[ \left( \frac{1-\sqrt{\epsilon}}{\sqrt{\epsilon}} \right) \left[ a^2 \left[ (n/\mathrm{NA})^2 - 1 \right] + \frac{1.49(M+1)^2 \lambda_{\mathrm{em}}^2 \left[ (n/\mathrm{NA})^2 - 1 \right]^2}{4M^2} \right] \right]^{\frac{1}{2}}, \quad (3)$$

where $\lambda_{\mathrm{em}}$ is the emission wavelength of the particle, $n$ is the index of refraction of the immersion medium, $M$ is the lateral magnification, NA is the numerical aperture and $\epsilon$ is chosen to be 0.1 (Meinhart and Wereley 2003; Wereley and Meinhart 2005). Estimates for the region of particle detectability (Table 1) are comparable in magnitude to the depth of field of the objective (Inoue and Spring 1997).

The probability distribution for the initial position $z_0$ of any particle (measured from the center of the focal plane) is given by $P(z_0) = 1/2h$ assuming uniform detectability, while the final position, $P(z|z_0)$, after a time $\Delta t$ is given by Eq. 1 (see Fig. 1). The final positions of particles detected within the focal plane is

$$P(z, z_0) = P(z_0)P(z|z_0) = \frac{1}{2h\sqrt{2\pi}d} \exp\left[ -\frac{(z-z_0)^2}{2d^2} \right]. \quad (4)$$

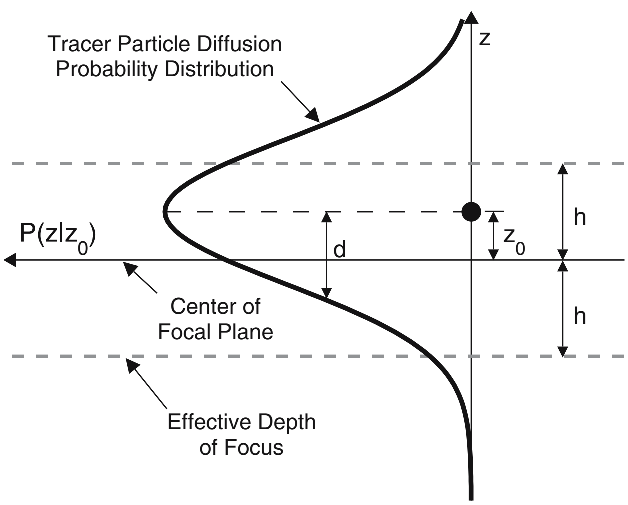


**Fig. 1** Diagram illustrating tracer particle diffusion along the optical axis, relative to the depth of field from an initial position $z_0$ to a final position $z$ after a time $\Delta t$. Out-of-plane drop-out results when the final position of a tracer is outside of the depth of field, $2h$

Integrating over the effective depth of field yields the probability, $P_{\perp,i}$, that a tracer particle initially in the depth of field will remain there after time $\Delta t$, while the out-of-plane drop-out probability is $P_{\perp,o} = 1 - P_{\perp,i}$. This can be expressed by the ratio between the focal plane depth and the diffusion length, $h/d$, and is shown in Fig. 2 (see Table 1 for typical values). Also shown are two typical $\mu$PIV operating conditions: a 300 nm particle in water imaged with a 60× objective, and a 6 nm QD with a 100× objective and fluid viscosity of water.

We can perform a similar analysis for the in-plane drop-out. For an asymmetric displacement distribution the most probable displacement is not necessarily the mean displacement, therefore, the distribution tails must be captured to completely quantify the distribution. In the case of pure diffusion, a square IR of side length $2l$ is constructed around the center of every particle in the first frame of an image pair. However, if a mean local velocity $\bar{u}$ is present, we assume that the IR is chosen sufficiently large to capture the tails of the distribution or appropriately shifted in the direction of the local velocity by an amount $\bar{u}\Delta t$ neither of which affect the shape of the spurious tracking distribution. For diffusion, the in-plane particle displacement is given by

$$P(x, y) = P(x)P(y) = \frac{1}{2\pi d^2} \exp\left[ -\frac{x^2 + y^2}{2d^2} \right]. \quad (5)$$

Equation 5 is integrated over the IR to yield the probability, $P_{\parallel,i}$, that a given particle will stay within

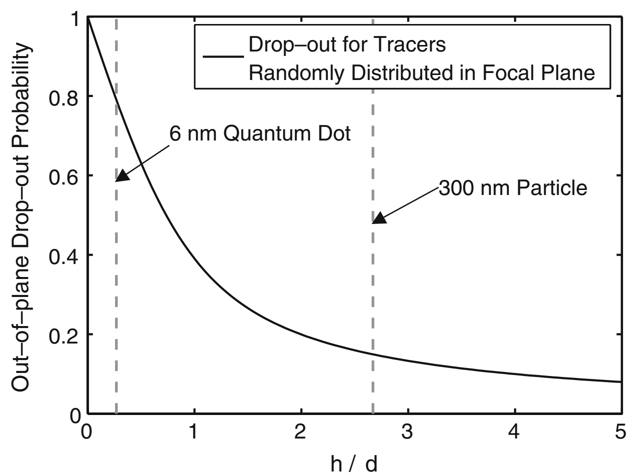


**Fig. 2** Out-of-plane tracer particle drop-out probability, where $h$ is the half-depth of the focal plane and $d$ is the diffusion length of the tracer particle. Also shown are two typical cases for $h/d$: a 300 nm particle in water imaged with a 60× objective, and a 6 nm quantum dot in water imaged with a 100× objective

the IR. Thus, the in-plane drop-out probability is $P_{\|,o} = 1 - P_{\|,i}$, which is shown in Fig. 3. We can choose $l/d \gg 1$ so that the in-plane drop-out probability is effectively zero. In practice, if we choose $l/d$ over 3, $P_{\|,o}$ will be less than 1% for diffusion and/or convection, when the tails of the displacement distribution are included, effectively eliminating in-plane drop-out. We point out that a 6 nm QD requires an IR side length seven times greater than a 300 nm particle for the same fluid conditions and exposure time. Combining the in-plane and out-of-plane drop-out, the total drop-out probability, $P_{\mathrm{drop}}$, is

$$P_{\mathrm{drop}} = 1 - P_{\perp,i} P_{\|,i}. \tag{6}$$

### 2.3 Statistical particle tracking procedure

Next, we describe the SPTV algorithm procedure and theory to predict contributions of spurious trackings. An image pair consists of two sequential CCD images (image A and image B with area $A_{\mathrm{image}}$). For each image pair, basic image processing techniques are first applied to eliminate defective pixels and other obvious noise signals. Following this, "signals" (i.e., potential particles) are identified through intensity thresholding. Next, the sub-pixel center locations of each signal are found through a $3 \times 3$ pixel, two-dimensional Gaussian fit. The Gaussian fit is used to approximate the diffraction limited spot produced by the sub-wavelength diameter particles and has been shown to be more accurate in determining particle displacements than correlation methods for single sub-wavelength particles (Cheezum et al. 2001). However, with the long exposure times typically used for low intensity probes, significant tracer motion can affect the accuracy of the Gaussian center detection method at low viscosities. An IR is defined around a single signal in image A according to the criteria set by Sect. 2. Displacements in $x$ and $y$ are computed from that single signal location in image A to any signal location in image B that falls into that IR. This process is repeated for each signal identified in image A, then a displacement distribution is constructed from the cumulative data. Additionally, displacements may be binned together for smaller sections of each image to resolve velocity gradients. However, the bins should be small enough so that the velocity is approximately constant in that region and several hundred images are typically needed to achieve proper statistical averaging. Finally, the spurious, uncorrelated trackings must be removed from the total displacement distribution. For the purposes of this paper, a Gaussian distribution was fitted to the distribution lineshape to extract the random, uniform distribution due to uncorrelated trackings.

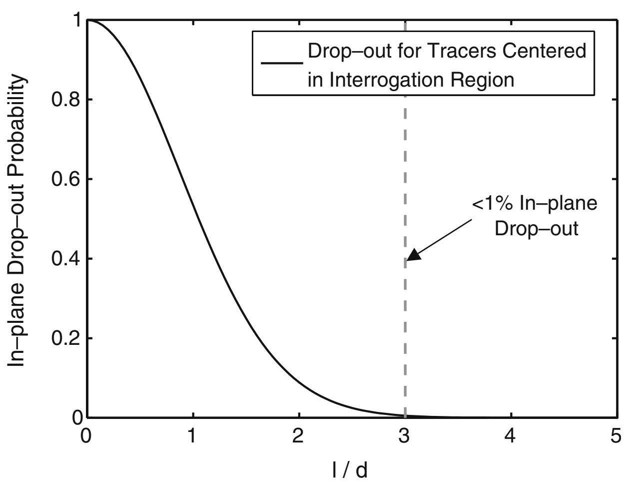


**Fig. 3** In-plane tracer particle drop-out probability where $l$ is the half-width of the interrogation region ($IR$) and $d$ is the diffusion length of the tracer particle. Choosing an IR greater than three times the particle diffusion length ensures to 99.5% probability that a particle originally centered in the IR will not drop out of the IR within the focal plane

In theory, the size of the uncorrelated tracking distribution can be determined if we know the both the drop-out probability and the number of real particles per image. The drop-out can be calculated from the theory outlined in Sect. 2. The number of real particles per image can be determined by carefully seeding the fluid, which is characterized by an area concentration, $c_{\mathrm{P}}$, due to the integration of the camera through the focal plane. For an image with area $A_{\mathrm{image}}$, the number of physical particle trackings is

$$N_{\mathrm{PP,phys}} = A_{\mathrm{image}} c_{\mathrm{P}} \left(1 - P_{\mathrm{drop}}\right), \tag{7}$$

where $P_{\mathrm{drop}}$ is the total drop-out probability, estimated from the system properties (Eqs. 1–6). The number of spurious trackings is given by ($N_{\mathrm{total}} - N_{\mathrm{PP,real}}$), where $N_{\mathrm{total}}$ is the total number of tracking found from the SPTV algorithm, which can now be subtracted from the total displacement distribution.

Furthermore, we can estimate the number of particle–noise, noise–particle and noise–noise trackings. The number of each contributing to the random displacement distribution is simply the number of one type of signal (particle or noise) found in image A multiplied by the expected number of another signal type found in an IR of image B. The resulting number of trackings are as follows:

$$N_{\mathrm{NP}} = A_{\mathrm{IR}} c_{\mathrm{P}} c_{\mathrm{N}} A_{\mathrm{image}}, \tag{8a}$$

$$N_{\mathrm{PN}} = A_{\mathrm{IR}} c_{\mathrm{N}} c_{\mathrm{P}} A_{\mathrm{image}}, \tag{8b}$$

$$N_{\mathrm{NN}} = A_{\mathrm{IR}} c_{\mathrm{N}}^2 A_{\mathrm{image}}, \tag{8c}$$

where $A_{\mathrm{IR}}$ is the area of the IR typically equal to $(2l)^2$. However, as mentioned in Sect. 2, the IR may be asymmetric and/or shifted without affecting the random, uniform distribution due to spurious trackings, as long as the shape and relative position is constant for an ensemble of trackings. The number of uncorrelated particle–particle trackings is calculated by subtracting the sum of these contributions from the total number of particle trackings

$$N_{\mathrm{PP,random}} = N_{\mathrm{total}} - \left(N_{\mathrm{PP,phys}} + N_{\mathrm{PN}} + N_{\mathrm{NP}} + N_{\mathrm{NN}}\right). \tag{9}$$

Estimations for the accuracy of the mean displacement (velocity) and diffusion length measurements are also derived from the statistics of the system. The standard error of the mean physical displacement is related to the standard deviation of the distribution, which is simply the diffusion length. For any displacement distribution, the true mean is contained within the 95% confidence interval of the measured mean with the well known factor $\pm 2d/\sqrt{N_{\mathrm{PP,phys}}}$ The standard error of the diffusion length measurement is more complex and for the general case depends on the fourth and second moments of the displacement distribution (Kendall and Stuart 1977). However, for a normal distribution, the 95% confidence interval for the standard error of the diffusion length reduces to $\pm d\sqrt{2/N_{\mathrm{PP,phys}}}$ A total of 1,000 physical trackings results in an error of approximately ±6.3%$d$ for the mean displacement and ±4.5%$d$ for the diffusion length.

### 2.4 Numerical validation

The SPTV algorithm was validated numerically using MATLAB to simulate particle and noise signal locations for particle diffusion. Random particle and noise signal locations were produced on a 2-D domain corresponding to an area several IRs larger than a typical image to allow for in-plane drop-in on the actual image domain. For a second domain, a fraction of the particle signals, proportional to $P_{\perp,i}$, were perturbed in the $x$ and $y$ direction according to a random, normal distribution with standard deviation $d$. For the remaining number of particles and noise signals, random signal locations were produced to emulate out-of-plane drop-in/drop-out and random generation of noise. Again, we

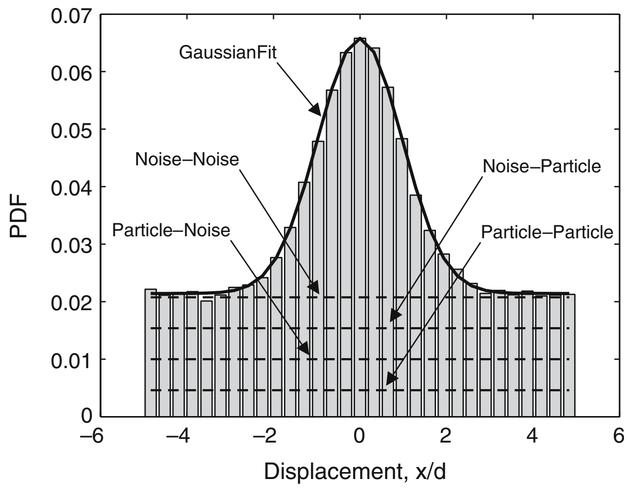


**Fig. 4** Displacement distribution for simulated diffusion data with intensifier noise and drop-in/drop-out. The cumulative contributions to the random distribution due to tracking noise and drop-out particles were calculated from the statistical tracking algorithm

assume that the probability of drop-out is the same as the drop-in. All signals were tracked using the SPTV algorithm described above in Eqs. 7, 8a, b, c and 9 for approximately 200 image pairs. Additionally, the exact contributions from tracer mismatching and random signal cross tracking were computed with the knowledge of the simulated signal origins. Cumulative contributions to the PDF from each type of tracking calculated by Eqs. 7, 8a, b, c and 9, which correspond closely to the exact values. A typical displacement distribution is shown in Fig. 4 for 50,000 total trackings resulting from 60% drop-out, 50% noise signals and a total signal concentration corresponding to an intersignal distance of 15 diffusion lengths. The ability of the equations to accurately predict the height of the uncorrelated floor is good confirmation that the basis of technique is sound.

## 3 Experimental validation

The tracking algorithm was also validated using three physical experiments. The experiments measured the diffusion and/or convection of three different tracer particles: 54 nm diameter FITC-Dextran molecules, 6 nm diameter organic-soluble QDs and 16 nm diameter water-soluble QDs. The images were acquired using a Nikon Eclipse TE2000-U inverted microscope with a Nikon PL Apo NA 1.45 100× TIRF oil immersion objective and an intensified CCD (ICCD) camera (Q-Imaging Intensified Retiga) capable of 1,360 pixels × 1,036 pixels 12-bit images with an effective pixel size of 64.3 nm at 100×. Tracers were illuminated using a mercury lamp 3–5 μm above the lower glass surface or through-the-objective total internal reflection fluorescence (TIRF) (Huang et al. 2006) with the 514.5 nm line of an argon ion laser (Coherent) within about 135 nm of the lower glass surface. The camera's intensifier gate was used to control the image exposure and a syringe pump (Harvard Apparatus) was used to charge the channels. Solvent viscosities were found using a TA Instruments AR-2000 Rheometer or specified tables. In-house MATLAB software was used for data acquisition and particle tracking.

### 3.1 SPTV using single molecule tracers

Free diffusion of fluorescein isothiocyanate-dextran (FITC-Dextran, 2,000,000 MW, Sigma-Aldrich) molecules in solution was observed between two cover glasses separated by 10 μm. The molecules have a hydrodynamic radius of 27 nm specified by manufacturer and peak absorption and emission wavelengths of 490 and 525 nm, respectively. The FITC-Dextran molecules were dissolved into a solvent of 33% pure water (Fluka) and 66% glycerol (99.5+%, Sigma-Aldrich) by volume with a dynamic viscosity of 24.3 cP at room temperature. Images were acquired with a 10 ms integration time and a 20 ms separation time between the frames of each image pair.

After measuring the total displacement distribution, the spurious displacements were estimated by fitting a Gaussian profile to the data. Figure 5 confirms this, and shows the Gaussian displacement distribution due to isotropic Brownian motion, sitting atop the random, uniform distribution resulting from spurious trackings

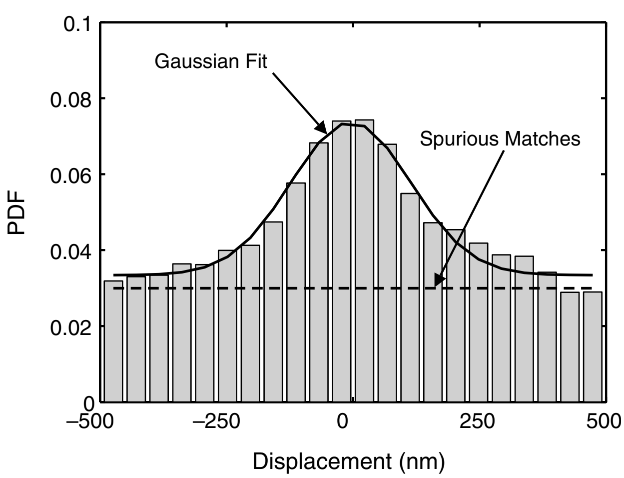


**Fig. 5** Measured displacement distribution for the free diffusion of 54 nm FITC-Dextran molecules in a glycerol/water solution with a viscosity of 24.3 cP

as determined by our analysis. For these particles and imaging system, the drop-out probability was about 50% and the ratio of physical trackings to spurious trackings was about 2 to 1 for about 5,000 trackings, which is mostly due to high levels of detectable noise signals. The measured diffusion length was $d_{PTV}$ = 133 nm, which compares well to the predicted Stokes–Einstein model of $d_{SE}$ = 115 nm with error possibly resulting from the high sensitivity of glycerol solutions to concentration and especially temperature.

### 3.2 SPTV using QDs

A more challenging application of the SPTV technique is found when using very small tracer particles. Quantum dots are semiconductor nanocrystals with monodispersed size, narrow emission spectra and broad absorption spectra. They show great promise for use as tracer particles in nanofluidic systems (Bausch and Weitz 2002; Pouya et al. 2005). However, QDs add another complication to the SPTV analysis. QDs exhibit well-known fluorescence intermittency or ‘‘blinking’’ (Nirmal et al. 1996; Shimizu et al. 2001) where, under continuous illumination, QDs cycle through states of nearly continuous emission and darkness. Within the context of particle tracking, blinking can be treated in a similar manner to drop-in/drop-out, although the statistics of this optical drop-out must be characterized experimentally. Methods for blinking suppression have been demonstrated (Hohng and Ha 2004), but blinking is actually a useful feature to differentiate single QDs from groups of aggregated QDs, if necessary. Pure (core or core-shell) QDs can only be used in organic solvents. Water-soluble QDs have an additional ligand coating, which increases their diameter and can decreases their emission intensity. The organic-soluble QDs used in this study were CdSe/ZnS core-shell QDs with a diameter of 6.1 nm (Evident Technologies, diameter determined by TEM) and a peak emission wavelength of 614 nm. The water-soluble QDs (Quantum Dot Corporation, diameter determined by a HPLC method) were also CdSe/ZnS core-shell QDs with a core diameter of about 6 nm and an overall hydrodynamic diameter of about 16 nm due to a carboxyl or amine coating to make them water-soluble and a peak emission wavelength of 606 nm.

#### 3.2.1 *Quantum dot blinking characteristics*

To quantify the nature of blinking, organic-soluble QDs in toluene were immobilized by drying a dilute solution on a glass coverslip, then covering them with another coverslip to minimize the effects of oxidation.

The blinking of several hundred single QDs was observed under continuous mercury lamp illumination for a period of 10 min. Images were recorded using an ICCD camera and locations of the QDs were identified and monitored in time. The signals were scaled by the background noise, which was normalized to have a mean and standard deviation of one. By defining an intensity threshold based on a signal to noise ratio (SNR) of about 5, we were able to designate on-times and off-times. A sample intensity time trace of a single blinking QD is shown in Fig. 6. The on-time and off-time blinking statistics were verified as previously reported by Shimizu et al. (2001) as an initial test for single QD detection. Histograms for the length of consecutive off-times and on-times (not shown here) exhibited the characteristic power law slope of –1.5 in excellent agreement with the results reported by Shimizu et al. (2001). The on-times also showed strong for deviation from the power law for long on-times.

For PTV applications, blinking characteristics are similar to drop-in and drop-out. If we assume that the QD is physically present in both frames of an image pair, then it is important to know if it will be optically ‘‘on’’ in both frames. This is a slightly different reading of the raw blinking statistics measured above. Single QD blinking was observed for different exposure times and inter-frame times in order to determine the blinking probability. Image pairs of immobilized QDs were recorded for exposure times varying from 1 to 50 ms and inter-frame times varying from 2 to 51 ms according to the same procedure outlined above. ‘‘On-states’’ and ‘‘off-states’’ were identified for each frame within an image pair. Both on- and off-times with time scales less than the camera exposure time can occur within a single exposure. The sensitivity of the detector and the SNR determine the ability to designate an on-state (or off-state) for a given frame. The probabilities for a single QD to be on in both frames (on–on), off in both frames (off–off), on in the first frame and off in the second (on–off) and off in the first frame and on in the second (off–on) were determined (Fig. 7). This data indicates that the image pair blinking probabilities are approximately invariant for exposure time and separation time under continuous illumination (not surprising given the low SNR chosen). Notice that about 70% of the QDs are in off-states during both frames of an image pair. This result is most likely due to the decay of QD emission intensity for prolonged exposure to illumination (Chung and Bawendi 2004). This result may change if pulsed or gated illumination is used, as is common in PTV systems, which use Q-switched or shuttered laser systems. Since these QDs are effectively invisible to a real PTV analysis, they have no effect on the blinking drop-out/drop-in probabilities. Of the detectable QDs, only those which remain on for two consecutive frames and remain within the interrogation volume will contribute to the physical tracer particle displacement distribution. From this data, the blinking drop-out and drop-in probability is calculated by

$$P_{\text{drop-out,blink}} = \frac{P_{\text{on-off}}}{P_{\text{on-off}} + P_{\text{on-on}}}, \tag{10a}$$

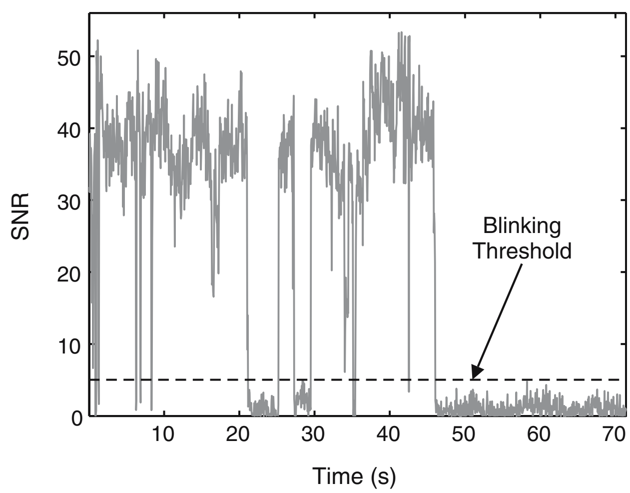


**Fig. 6** Sample intensity time trace for single, immobilized QDs under continuous illumination. An intensity greater than the threshold of SNR = 5 designates blinking on-times from off-times

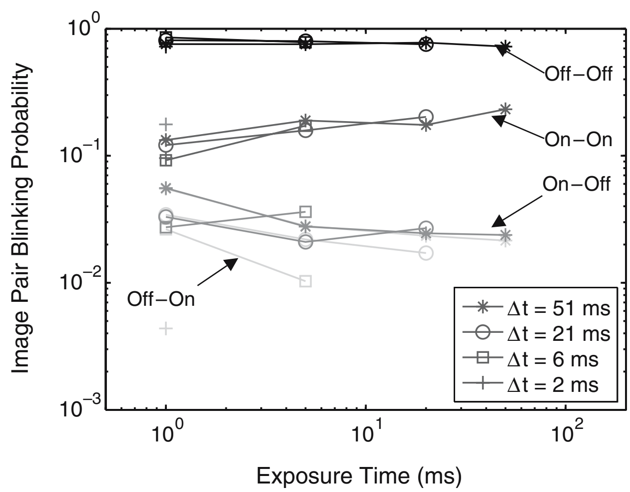


**Fig. 7** Quantum dot blinking probability for two successive images with varying exposure time and inter-frame time. Only QDs that are ‘‘on’’ in both frames are trackable, while QDs that are ‘‘on’’ in only one frame optically drop-in or drop-out with a probability of about 12%. The QDs that are ‘‘off’’ in both frames of an image pair are essentially invisible and untrackable

$$P_{\text{drop-in,blink}} = \frac{P_{\text{off-on}}}{P_{\text{off-on}} + P_{\text{on-on}}} \tag{10b}$$

where $P_{\text{drop-out,blink}} \approx P_{\text{drop-in,blink}}$ as expected. Physically, these quantities represent the probability of observing the transition of a QD from an on-state to an off-state within an image pair, which is about 12%. We should note that the optical drop-out is much less than the physical drop-out of a QD in a water-like substance (≈80%). The blinking drop-out probability is combined with the diffusion drop-out to yield the total drop-out probability. So, we see that the for tracer particles with high drop-out, the effects of blinking on tracer particle detectability diminish.

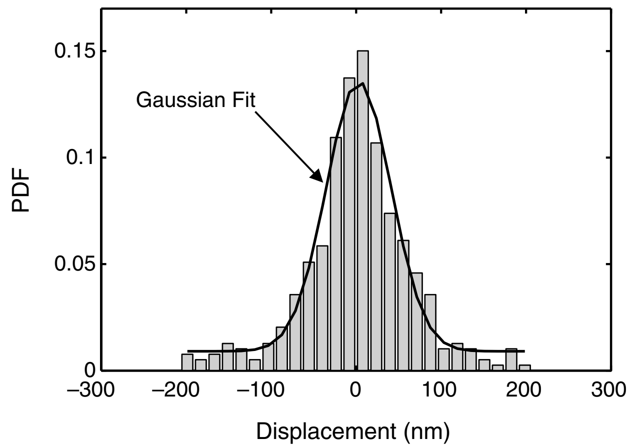


**Fig. 9** Measured displacement distribution for the free diffusion of 6 nm QDs in a hexane/PDMS solution with a viscosity of 413 cP

### 3.2.2 *Diffusion measurements using organic-soluble QDs*

Free diffusion of 6.1 nm organic-soluble QDs was observed with mercury lamp illumination in a sealed Poly(dimethylsiloxane) (PDMS) microchannel. For this demonstration, the solvent viscosity and exposure time was chosen to ensure that single QDs were captured both blinking and diffusing. The QDs were resuspended in 13% hexane and 87% 1000 cSt PDMS 200 fluid (Sigma-Aldrich) with a viscosity of 413 cP at room temperature. The camera exposure was set to a 15 ms integration time with a separation time of 20 ms between the frames of each image pair. A sample time sequence of evenly spaced images for a single, blinking QD is shown in Fig. 8.

The distribution of the QD displacements is shown in Fig. 9 and reveal some interesting characteristics. Firstly, the general character of the distribution is similar to that found in the FITC-Dextran tracers. The characteristic uncorrelated tracking floor was also predicted as before and was quantified by fitting a Gaussian distribution to the data of 3,000 total trackings. However, on close examination, the width of the diffusion distribution ($d_{\text{PTV}}$ = 42 nm) is smaller than would be predicted using the idealized Stokes–Einstein model ($d_{\text{SE}}$ = 83 nm) with the known QD diameter and the measured viscosity of the solvent. Although we do not know the source of this reduced diffusion, there are two possibilities. The first is that the QDs were not single dots, but aggregations with larger effective radii. However, since blinking was observed, this is considered an unlikely explanation. A second possibility is that the QDs are diffusing through a network of long-chain PDMS molecules whose average chain length (121 nm) is significantly larger than the QD diameter (6 nm). This larger-scale network likely leads to non-Brownian diffusion (Lin and Phillies 1984; Cheng et al. 2002) although detailed study of this is beyond the

**Fig. 8** Quantum dot images: **a** a composite time series of seven frames with equal time spacing for an organic soluble QD diffusing and blinking in a slight convective flow in PDMS and hexane (6.5 μm × 6.5 μm field of view) and **b** typical image of QDs in water illuminated by an evanescent field (19.3 μm × 19.3 μm field of view)

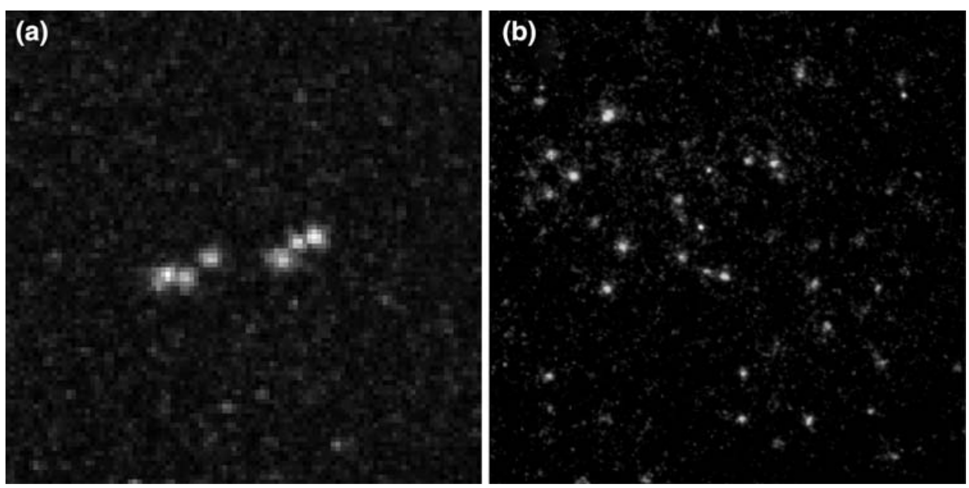

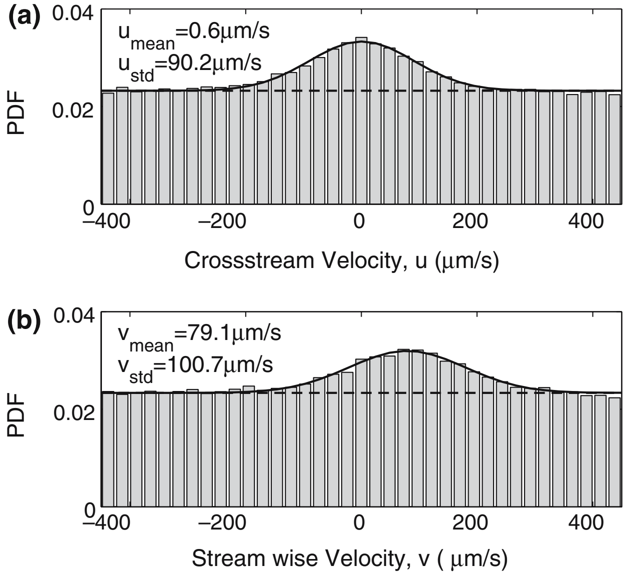


**Fig. 10** Measured velocity distributions for 16 nm carboxyl conjugated water-soluble QDs in a water-based buffer solution in the **a** cross-stream and **b** streamwise directions for a PDMS microchannel using TIRF with the SPTV algorithm for 900 image pairs

scope of the current manuscript which focuses solely on the particle tracking demonstration and use of nanometer-sized tracers.

### *3.2.3 Velocity measurements using water-soluble QDs*

Carboxyl coated water-soluble QDs in a water-based buffer with a 16 nm hydrodynamic diameter were imaged flowing in a rectangular 75 μm × 600 μm PDMS micro-channel within 135 nm of the surface using the TIRF method described above. The high SNR of the TIRF method along with a high power argon ion laser and ICCD camera allowed for camera exposures as low as 1 ms. A typical TIRF image of the QDs in buffer is shown in Fig. 8. Diffusion measurements using the SPTV method at inter-frame times of 3 and 7 ms showed a mean diffusivity of 16.7 $\mu m^2/s$.

The QDs were also tracked in both the streamwise and cross-stream directions for various flow rates using the SPTV algorithm with an inter-frame time of 4 ms. An example is shown in Fig. 10. The data again shows diffusion dynamics atop a random, uniform distribution with over 140,000 total trackings and a ratio of physical trackings to spurious trackings of about 1 to 10 resulting from 900 image pairs. The high diffusivity and shallow imaging depth contribute to the significant drop-out and particle mismatching. A mean displacement shift in the streamwise direction corresponds to measured mean velocities, $v_{mean}$, of 34.8, 79.1 and 139.1 μm/s for flow rates of 10, 20 and 40 $\mu$L/min, respectively, and less than 5 μm/s cross-stream velocity, $u_{mean}$. An increasing standard deviation of velocity in the streamwise direction, $v_{std}$, of 90.6, 100.7 and 110.9 μm/s was observed with increasing flow rate, while the standard deviation of velocity in the cross-stream direction, $u_{std}$, remained nearly constant with a mean of 91.7 μm/s (consistent with the diffusivity measured above). This is attributed to sampling different shear planes within the evanescent field where the streamwise velocity varies away from the wall (Huang et al. 2006). Finally, hydrodynamic interactions between the particle and wall hinder the 118.7 μm/s standard deviation predicted by the Stokes–Einstein model to 111.0 μm/s (Lin et al. 2000), which is consistent with a slightly larger nominal tracer diameter than the hydrodynamic diameter specified by the manufacturer.

To resolve velocity fields with the SPTV technique, particle trackings are binned together within an image and the analysis is performed as described earlier. In Fig. 11, we show an example of a flow near a corner in a 10 μm deep PDMS micro-channel for amine coated

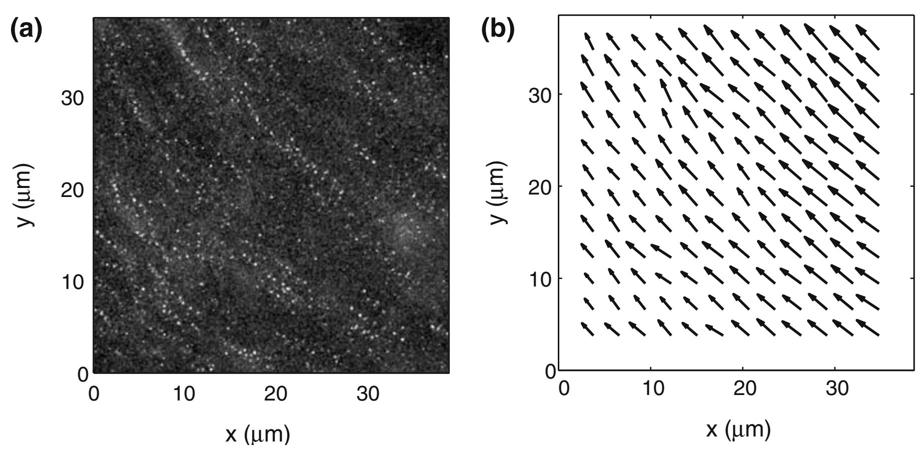


**Fig. 11** Amine conjugated water-soluble quantum dot seeded flow near a corner in a micro-channel: **a** composite of ten equally spaced images and **b** the corresponding vector field computed with the SPTV method. The vectors are the result of binning particle displacements over a 5.7 μm (88 pixels) square window with 50% overlap for 800 image pairs

**Table 1** Properties for typical tracer particle/fluid systems

| Particle | Fluid | Wavelength $\lambda_{em}$ (nm) | Diameter $2a$ (nm) | Viscosity $\mu$ (cP) | Diffusion length $d$ (nm) | Focal plane $2h$ (nm) | Ratio $h/d$ |
|---|---|---|---|---|---|---|---|
| Microsphere | Water | 612 | 500 | 0.9 | 87 | 630 | 3.60 |
| Microsphere | Water | 612 | 200 | 0.9 | 138 | 469 | 1.70 |
| FITC-Dextran | Glycerol and water | 525 | 54 | 24.3 | 115 | 177 | 0.77 |
| Quantum dot | Toluene | 614 | 6.1 | 0.6 | 2,150 | 130 | 0.03 |
| Quantum dot | Hexane and PDMS | 614 | 6.1 | 413 | 83 | 292 | 1.77 |
| Quantum dot | Water | 606 | 16 | 0.9 | 489 | 427 | 0.44 |
| Quantum dot | Glycerol and water | 606 | 16 | 50 | 147 | 201 | 0.69 |

water-soluble QDs in a 50 cP glycerol solution (Sheely 1932). Each vector is the result of approximately 7,500 trackings over a 5.7 μm (88 pixel) square window with 50% overlap and a ratio of physical to random trackings of 1 to 3. To achieve a sufficient number of physical trackings, 800 image pairs were needed for proper averaging, which yielded a mean velocity of 4.4 μm/s over the domain. We do note that aggregations can occur in systems with high concentrations of QDs and glycerol, however, this does not affect our ability to measure mean velocities.

## 4 Conclusions

We have identified several shortcomings of traditional particle tracking techniques that become important as the tracer particles become smaller. The statistical particle tracking velocimetry (SPTV) algorithm presented here addresses many problems associated with small tracers, including the desire to use higher tracer seeding densities, large drop-out rates and the fluorescence intermittency behavior of QDs. However, effects of fluorescence intermittency are diminished in comparison to physical drop-out in highly diffusive systems. The essential approach of the SPTV algorithm is to measure displacement distributions, rather than single displacements, and to use the known statistics of the system to eliminate random signal trackings due to trackable intensifier noise signals, tracer mismatching and drop-in/drop-out.

The algorithm has been verified using both simulations and experiments and shows great promise as a velocimetry technique for nanometer-sized tracer particles in systems with significant intensifier noise and with large tracer particle diffusivities and concentrations. In the present paper, we have validated the SPTV algorithm for several systems employing innovative tracer particles: single molecules and quantum dots, but the technique is also applicable over the full range of tracer particle length scales where traditional $\mu$PIV and $\mu$PTV methods are typically used. By treating all detectable signals within an image equally, the underlying physics of the system is allowed to present itself, while the uncorrelated information is easily removed through simple statistics. It is this simplicity that makes the statistical tracking algorithm attractive for smaller length scales. However, there is still much room for improvement in nano-PIV/PTV systems.

Lastly, we have observed a smaller measured diffusion length as compared to the expected Stokes–Einstein prediction for both the organic and inorganic QDs. In the case of the organic QDs, the smaller diffusion dynamics may be the result of diffusion in a long-chain liquid polymer. However, the similar discrepancy, to a lesser extent for the water-soluble QDs suggests that the small size of the tracers may not be accurately described by the Stokes–Einstein relation, even when taking into account hindered diffusion where applicable, but we cannot completely explain this phenomenon. The unexpected width of the diffusion peak has no impact on the ability of the SPTV technique to measure mean velocities in micro- and nano-fluidic systems, but only on the interpretation of the distribution shape. For example, it has been proposed (Wereley and Meinhart 2005) that the width of the distribution could be used to measure local fluid temperature. Although this is an appealing idea, it is fraught with complexities of the type revealed here, since complex fluids and small tracer particles are not guaranteed to observe the Stokes–Einstein relation. Similarly, in shear flows, the displacement (and hence velocity) distributions can be non-Gaussian (Huang et al. 2006) and so it becomes critical to measure the distributions and not to assume any particular shape.

**Acknowledgments** This research was supported by Sandia National Laboratories through a joint SNL/NSF research program, and by Physical Sciences Incorporated, through a USAF STTR program.

## References


Adrian RJ (1991) Particle imaging techniques for experimental fluid mechanics. Annu Rev Fluid Mech 23:261–304

Bausch AR, Weitz DA (2002) Tracking the dynamics of single quantum dots: beating the optical resolution twice. J Nanoparticle Res 4:477–481

Breedveld V, van den Ende D, Acrivos ATA (1998) The measurement of the shear-induced particle and fluid tracer diffusivities in concentrated suspensions by a novel method. J Fluid Mech 375:297–318

Burke MW (1996) Image acquisition, 1st edn. Chapman and Hall, London, chap 5

Cheezum MK, Walker WF, Guilford WF (2001) Quantitative comparisons of algorithms for tracking single fluorescent particles. Biophys J 81:2378–2388

Cheng Y, Prud'homme RK, Thomas JL (2002) Diffusion of mesoscopic probes in aqueous polymer solutions measured by fluorescence recovery after photobleaching. Macromolecules 35:8111–8121

Chung I, Bawendi MG (2004) Relationship between single quantum dot intermittency and fluorescence decays from collections of dots. Phys Rev B 70:2897–2902

Hohng S, Ha T (2004) Near-complete supression of quantum dot blinking in ambient conditions. J Am Chem Soc 126:1324–1325

Huang P, Guasto JS, Breuer KS (2006) Direct measurement of slip velocities using 3-d total internal reflection velocimetry. J Fluid Mech 566:447–464

Inoue S, Spring KR (1997) Video microscopy: the fundamentals, 2nd edn. Plenum Press, New York

Jin S, Huang P, Park J, Yoo JY, Breuer KS (2004) Near-surface velocimetry using evanescent wave illumination. Exp Fluids 37:825–833

Kendall M, Stuart A (1977) The advanced theory of statistics, vol 1, 4th edn. Macmillan, New York, chap 10

Lin TH, Phillies GD (1984) Probe diffusion in poly(acrylic acid)-water. Effect of probe size. Macromolecules 17:1686–1691

Lin B, Yu J, Rice SA (2000) Direct measurements of constrained brownian motion of an isolated sphere between two walls. Phys Rev E 62:3909–3919

Meinhart CD, Wereley ST (2003) The theory of diffraction-limited resolution in microparticles image velocimetry. Meas Sci Technol 14:1047–1053

Nirmal M, Dabbousi BO, Bawendi MG, Macklin JJ, Trautman JK, Harris TD, Brus LE (1996) Fluorescence intermittency in single cadmium selenide nanocrystals. Nature 383:802–804

Pouya S, Koochesfahani M, Snee P, Bawendi M, Nocera D (2005) Single quantum dot (qd) imaging of fluid flow near surfaces. Exp Fluids 39:784–786

Schmidt T, Schutz GJ, Baumgartner W, Gruber HJ, Schindler H (1996) Imaging of single molecule diffusion. Proc Natl Acad Sci USA 93:2926–2929

Sheely ML (1932) Glycerol viscosity tables. Ind Eng Chem 24:1060–1064

Shimizu KT, Neuhauser RG, Leatherdale CA, Empedocles SA, Woo WK, Bawendi MG (2001) Blinking statistics in single semiconductor nanocrystal quantum dots. Phys Rev B 63:1–5

Wereley ST, Meinhart CD (2005) Microscale diagnostic techniques. Springer, Berlin Heidelberg New York, chap 2